Published in final edited form as:
Proteomics. 2009 March ; 9(5): 1314–1325. doi:10.1002/pmic.200800718.

Proteomic profiling of K_{ATP} channel-deficient hypertensive heart maps risk for maladaptive cardiomyopathic outcome

Jelena Zlatkovic[1], **D. Kent Arrell**[1], **Garvan C. Kane**[1], **Takashi Miki**[2], **Susumu Seino**[3], and **Andre Terzic**[1]

[1] Marriott Heart Disease Research Program, Division of Cardiovascular Diseases, Departments of Medicine, Molecular Pharmacology & Experimental Therapeutics, and Medical Genetics, Mayo Clinic, Rochester, MN, USA

[2] Department of Autonomic Physiology, Graduate School of Medicine Chiba University, Chiba, Japan

[3] Division of Cellular and Molecular Medicine, Kobe University Graduate School of Medicine, Kobe, Japan

Abstract

KCNJ11 null mutants, lacking Kir6.2 ATP-sensitive K^+ (K_{ATP}) channels, exhibit a marked susceptibility towards hypertension (HTN)-induced heart failure. To gain insight into the molecular alterations induced by knockout of this metabolic sensor under hemodynamic stress, wild-type (WT) and Kir6.2 knockout (Kir6.2-KO) cardiac proteomes were profiled by comparative 2-DE and Orbitrap MS. Despite equivalent systemic HTN produced by chronic hyperaldosteronism, 114 unique proteins were altered in Kir6.2-KO compared to WT hearts. Bioinformatic analysis linked the primary biological function of the K_{ATP} channel-dependent protein cohort to energetic metabolism (64% of proteins), followed by signaling infrastructure (36%) including oxido-reductases, stress-related chaperones, processes supporting protein degradation, transcription and translation, and cytostructure. Mapped protein–protein relationships authenticated the primary impact on metabolic pathways, delineating the K_{ATP} channel-dependent subproteome within a nonstochastic network. Iterative systems interrogation of the proteomic web prioritized heart-specific adverse effects, *i.e.*, “Cardiac Damage”, “Cardiac Enlargement”, and “Cardiac Fibrosis”, exposing a predisposition for the development of cardiomyopathic traits in the hypertensive Kir6.2-KO. Validating this maladaptive forecast, phenotyping documented an aggravated myocardial contractile performance, a massive interstitial fibrosis and an exaggerated left ventricular size, all prognostic indices of poor outcome. Thus, Kir6.2 ablation engenders unfavorable proteomic remodeling in hypertensive hearts, providing a composite molecular substrate for pathologic stress-associated cardiovascular disease.

Keywords

ATP-sensitive K^+ channel; Bioinformatics; Heart failure; Kir6.2; Systems biology

Correspondence: Dr. Andre Terzic, Mayo Clinic, Stabile 5, 200 First Street SW, Rochester, MN 55905, USA, E-mail: terzic.andre@mayo.edu, Fax: + 1-507-266-9936.

The authors have declared no conflict of interest.

1 Introduction

Systemic HTN is a leading risk factor in the development of cardiomyopathy and heart failure [1–3]. The adverse cardiac manifestations of HTN encompass ventricular enlargement, interstitial fibrosis, and ultimately organ dysfunction, significantly contributing to morbidity and mortality in the population at large [4–6]. Heart adaptation to hypertensive stress load is however highly variable, with only certain individuals progressing from a state of risk to one of overt disease [7]. Homeostatic processes that ensure stress tolerance are only partially understood [8,9], warranting elucidation of individual cardioprotective components and their underlying systems organization within the hypertensive myocardium.

A prototypic stress-response element is the ATP-sensitive K^+ (K_{ATP}) channel, formed through heteromeric assembly of the inwardly rectifying K^+channel, Kir6.x, with the regulatory ATP-binding cassette sulfonylurea receptor protein [10–13]. The *KCNJ11* gene encodes the pore-forming Kir6.2 isoform of cardiac K_{ATP} channels, particularly abundant in the sarcolemma of ventricular myocytes [14–16]. K_{ATP} channels act as high-fidelity molecular rheostats, adjusting membrane potential-dependent functions to match energetic demands of the working heart [17,18]. Established in both experimental models and in humans, intact Kir6.2 is required for securing cardiac stress adaptation, with K_{ATP} channel malfunction implicated in the development of heart disease [19–21]. It has recently been recognized that a deficit in K_{ATP} channels impairs tolerance to systemic stressors, ranging from sympathetic surge [22–26] and endurance challenge [27] to hemodynamic load [28–30]. Moreover, genetic disruption of K_{ATP} channels compromises the protective benefits of preconditioning [31–33], while overexpression of channel subunits generates a resistant phenotype [34].

Cardioprotective properties of K_{ATP} channels have been linked to a tight integration of channel proteins with the cellular metabolic infrastructure, ensuring effective coupling of channel function with bioenergetic dynamics [35–41]. K_{ATP} channel subunits have been reported to physically associate and/or communicate with myocardial energy shuttles, *i.e.*, creatine kinase, adenylate kinase, and lactate dehydrogenase, and energy production pathways catalyzed by glycolytic or fatty acid biosynthesis enzymes, including glyceraldehyde-3-phosphate dehydrogenase, triosephosphate isomerase, and long chain acyl-CoA dehydrogenase [42–46]. Privileged channel interactions with identified partners have been implicated in cellular protection, whereas dysfunction of – or uncoupling from – interacting partners predisposes to stress intolerance [47–49]. Although present knowledge indicates that the K_{ATP} channel is integrated with cell metabolism, contributing to stress tolerance, a broader understanding of the channel's relationship with the cellular milieu and its implication on disease predisposition is currently lacking.

Indeed, biological functions can rarely be attributed to individual molecules, but rather arise through complex interactions between numerous cellular constituents [50–52]. Proteomic analysis provides a high-throughput, unbiased approach for large scale identification of proteins responsible for the execution of physiological processes [53]. As such, proteomic methodology is suited for dissecting the molecular fingerprint of K_{ATP} channel-dependent system associations. In the setting of HTN, the consequences of myocardial K_{ATP} channel deficiency were here examined by comparative 2-DE followed by nanoelectrospray linear IT tandem MS (nESI LC-MS/MS). Over one hundred identified proteins were differentially expressed within the cytosol of K_{ATP} channel knockouts compared to their WT counterparts. Bioinformatic examination of protein–protein relationships further mapped the primary impact on metabolic pathways, delineating that the K_{ATP} channel-dependent subproteome resides within a nonstochastic network. Stratification of the resolved interactome unmasked, in the absence of K_{ATP} channel function, a maladaptive predilection for cardiomyopathic traits under the stress of HTN. This proteomic approach thereby provides a systems-based diagnostic tool

to chart the composite molecular substrate of K_{ATP} channel deficiency in the hypertensive heart.

2 Materials and methods

2.1 Volume overload hypertension model

Protocols were carried out in accordance with NIH guidelines, following approval of the Mayo Clinic Institutional Animal Care and Use Committee. K_{ATP} channel Kir6.2 knockout (Kir6.2-KO) mice, generated by disruption of the *KCNJ11* gene encoding the Kir6.2 channel pore [54], were back-crossed for five generations to a C57BL/6 background. Targeted Kir6.2 disruption generates null mutants with ventricular myocytes lacking functional K_{ATP} channels [55]. Adult male C57BL/6 wild-type (WT) mice and age-matched male Kir6.2-KO counterparts underwent left nephrectomy through a retroperitoneal flank excision under isoflurane anesthesia to reduce urinary clearance. Mineralocorticoid-HTN was induced by subcutaneous implantation of a 50 mg 21 day release deoxycorticosterone-acetate tablet (Innovative Research of America) and supplementation with 1% NaCl plus 0.2% KCl in drinking water [28]. Mice were given standard rodent chow, and housed individually under a 12 h day/night cycle. Water and salt intake were measured weekly. Mice had similar nonfasting glycemic levels measured by tail sampling (OneTouch Ultra, Lifescan). Following one week of acclimatization training to restraint, blood pressure was measured by automated tail-cuff recording (Columbus Instruments) in awake restrained animals, two weeks post-nephrectomy. Blood pressure values were digitally derived from ten sequential recordings, documenting overt HTN in all WT and Kir6.2-KO by 14 days of mineralocorticoid/salt loading [28].

2.2 Protein extraction and quantitation

At 21 days, hypertensive WT and Kir6.2-KO animals were weighed, sacrificed under isoflurane anesthesia, and hearts excised and rinsed in PBS. Left ventricles including septum were removed, weighed *ex vivo*, snap-frozen in liquid N_2, and stored at −80°C. Cytosolic tissue extracts were prepared by mechanical homogenization at 4°C in four volumes of extraction buffer, consisting of (in mM) HEPES 25 (pH 7.4), PMSF 0.25, and DTT 50, 1.25 μM pepstatin A, Mini-Complete™ protease inhibitor cocktail (Roche Applied Science), and 1% phosphatase inhibitor cocktails 1 and 2 (Sigma) [56]. Samples were centrifuged (16 000×*g*) at 4°C for 10 min, supernatants were transferred to fresh tubes, and protein was quantified in triplicate by BioRad protein assay using the microassay procedure with a bovine gamma globulin standard [57,58].

2.3 2-DE and gel imaging

Protein extracts (100 μg) were resolved by IPG 2-DE following addition to IEF rehydration buffer (7 M urea, 2 M thiourea, 2% w/v CHAPS, 50 mM DTT, 1x BioRad pH 3–10 ampholytes). IPG Ready Strips™ (pH 3–10, 170 mm, BioRad) were actively rehydrated at 50 V for 10 h, followed by rapid voltage ramping with a series of 15 min steps at 100, 500, and 1000 V, and a final step at 10 000 V for 60 kVh at 20°C. Focused IPG strips were rinsed with distilled, deionized water, and incubated for 15 min in equilibration buffer (50 mM Tris-HCl, pH 8.8, 6 M urea, 30% v/v glycerol, 2% w/v SDS) containing 10 mg/mL DTT, followed by 15 min in equilibration buffer containing 25 mg/mL iodoacetamide. After horizontal positioning on 12.5% SDS–PAGE gels, strips were overlaid with SDS buffer (25 mM Tris, 192 mM glycine, 0.1% w/v SDS) containing 0.5% w/v agarose, and resolved orthogonally by SDS–PAGE in a Protean® II XL system (BioRad). Resolved 2-D gels were silver stained and digitized at 400 dpi for spot image analysis, including spot detection, matching, normalization, and quantification, conducted with BioRad PDQuest v.7.4.0 [58,59]. Individual gel images were normalized by total intensity of valid spots. Fold change was calculated as the [mean Kir6.2-KO]:[mean WT] ratio for protein spots increasing, or the negative inverse for protein

species decreasing, in K_{ATP} channel knockouts. For proteins identified in more than one spot, the sum of values for all spots was used to determine a weighted average treatment ratio, unless otherwise indicated.

2.4 Nanoelectrospray linear IT tandem MS

Significantly altered protein species were isolated, destained, and prepared for LC-MS/MS by reduction, alkylation, tryptic digestion, peptide extraction, and drying [59,60]. Peptides were reconstituted in 0.15% formic acid, 0.05% TFA, and trap injected onto a 75 μm × 10 cm ProteoPep C18 PicoFrit™ nanoflow column (New Objective). Chromatography was performed using 0.2% formic acid in solvents A (99% water, 1% ACN) and B (80% ACN, 5% isopropanol, 15% water), with peptides eluted over 30 min with a 5–45% solvent B gradient using an Eksigent nanoHPLC system (MDS Sciex) coupled to an LTQ-Orbitrap mass spectrometer (Thermo Fisher Scientific). Continuous scanning of eluted peptide ions was carried out between 375–1600 *m*/z, automatically switching to MS/MS CID mode on ions exceeding an intensity of 8000. Raw MS/MS spectra were converted to.dta files using Bioworks 3.2 (Thermo Fisher Scientific), and merged files matching +1, 2, or 3 peptide charge states were correlated to theoretical tryptic fragments in Swiss-Prot (v.53.0) using Mascot™ v.2.2 [61]. Searches were conducted on mammalian sequences (53 539 entries), tolerating up to two missed cleavages, a mass tolerance of ±0.01 Da for precursor ions (including ^{13}C peak detection) and ±0.6 Da for MS/MS product ions allowing for protein N-terminal acetylation, methionine oxidation, and cysteine carbamidomethylation. Protein identities were confirmed by matching multiple peptide spectra at $p<0.05$, with proteins accepted at $p<0.01$. Proteins identified by a single peptide were subjected to a higher stringency level ($p<0.01$), and were confirmed by manual spectrum inspection with detected fragment ions from the MS/MS spectrum required to be above baseline noise, have demonstrable continuity in b- or y-ion series, and proline residues yielding intense y-ions [62]. Protein assignments were further validated by congruence of observed *versus* predicted p*I*/M_r, using the ExPASy p*I*/M_r tool (http://us.expasy.org/tools/pi_tool.html), taking into consideration protein processing and PTMs [59].

2.5 Interactome network analysis

Differentially expressed proteins, with fold change ratios, were submitted as focus proteins for network analysis using Ingenuity Pathways Knowledge Base (Ingenuity® Systems, www.ingenuity.com) to identify associated functional networks. An overview of interactions was obtained by merging functional subnetworks into a composite interactome. The composite was depicted using the molecular interaction network visualization program Cytoscape 2.5.1, with topological properties characterized as an undirected network using Network Analyzer [63]. Computed properties included node degree (k), the number of links connected to the node, and node degree distribution (P[k]), the probability that a specified node has k links, defined as P[k] = X[k]/n, where X[k] is the number of nodes with degree k and n is the total number of network nodes [64,65]. P[k] *versus* k discriminates between random and scale-free topographies, defined by normal and power law distributions, respectively [64]. The Anderson–Darling normality test [66] ruled out a normal distribution, so P[k] *versus* k was calculated as a power law relationship using a cumulative distribution function [67] to determine γ in the power law distribution (P[k] ~ $k^{-\gamma}$) according to Eq. (1)

$$\gamma = 1 + n\left[\sum_{i=1}^{n} \ln \frac{x_i}{x_{min}}\right]^{-1} \quad (1)$$

where γ is the power law exponent, n the number of networknodes, x_i node degree, and x_{min} is the minimum node degree within the network, with statistical error σ [67] for Eq. (1) defined by Eq. (2)

$$\sigma = \sqrt{n}\left[\sum_{i=1}^{n} \ln \frac{x_i}{x_{min}}\right]^{-1} = \frac{\gamma - 1}{\sqrt{n}} \quad (2)$$

To link expression data with predicted pathological outcomes, the resolved network was interrogated with Ingenuity Pathways Analysis by screening for associated toxicity functions.

2.6 Cardiac function and structure

Prior to and following the 21 day HTN protocol, *trans*-thoracic echocardiography (Model c256 with a 15L8 probe, Acuson) was performed in lightly anesthetized (1.25% isoflurane) WT and Kir6.2-KO mice. Images were digitally acquired and stored for offline blinded analysis. Stroke volume was determined by the product of aortic root cross-sectional area and the velocity time integral taken from peak *trans*-aortic Doppler tracings [29,30]. The product of stroke volume and heart rate, expressed as mL/min, was used to calculate cardiac output [29]. Interstitial fibrosis was quantified by computer analysis (MetaMorph, Visitron Universal Imaging) of 0.5 μm thick, paraffin-embedded, Sirius red stained sections.

2.7 Statistical analysis

Comparison between groups was performed using a standard *t*-test of variables with 95% confidence intervals, with data expressed as mean±standard error.

3 Results

3.1 K_{ATP} channel knockout alters cardiac proteome in hypertension

Systemic HTN is a common condition of stress faced by the heart [9] with chronic hyperaldosteronism a leading cause [68], replicated herein through unilateral nephrectomy and mineralocorticoid/salt challenge (Fig. 1A). Sustained hemodynamic stress produced comparable HTN in WT and K_{ATP} channel knockout (Kir6.2-KO) mice (Fig. 1B). At 14 days of follow-up, systolic blood pressure increased significantly from 112 ± 5 to 137 ± 5 mm Hg in WT (n = 14, p<0.05), and similarly from 110 ± 4 to 135 ± 5 mm Hg in age-matched mice lacking the *KCNJ11*-encoded Kir6.2 channel pore (n = 12, p<0.05 compared to baseline and p = 0.8 when compared to WT). To assess the molecular consequences of K_{ATP} channel disruption, the left ventricular cytosolic proteome was extracted from WT (n = 4) and Kir6.2-KO (n = 5) hearts and profiled by comparative 2-DE (Fig. 1C). In broad pH range (pH 3–10) silver-stained gels, more than 900 protein species were consistently resolved. Reproducibility was documented by a high degree of correlation (R^2 = 0.922) between protein spot intensities from WT and Kir6.2-KO gels (Fig. 1D). Densitometric quantification demonstrated that a subset of 81 unique protein spots (9% of the total) was significantly altered in response to Kir6.2 deletion, 56 of which were downregulated and 25 upregulated (Fig. 1E). Thus, comparative expression profiling of WT and Kir6.2-KO myocardium revealed that, in response to equivalent hypertensive stress, the absence of functional K_{ATP} channels translates into a distinct, remodeled cardiac subproteome.

3.2 Mapping the Kir6.2-dependent subproteome

To characterize the K_{ATP} channel-dependent subproteome in the setting of HTN, a discriminatory analysis was carried out by LTQ-Orbitrap MS/MS contrasting WT *versus*

Kir6.2-KO. As examples of this multistep identification approach, spots 40 and 67 (Fig. 1C and enlarged in Fig. 2A, left insets), both down-regulated in the Kir6.2-KO dependent subproteome (Fig. 2A, right insets), were identified by MS/MS spectral peptide assignments as creatine kinase M (Fig. 2A, upper spectrum and peptide sequence) and adenylate kinase 1 (Fig. 2A, lower spectrum and peptide sequence) isoforms. These prototypic phosphotransfer enzymes have been demonstrated to couple cellular bioenergetics with K_{ATP} channel activity [42,43,47]. Indeed, metabolic enzymes with previously recognized associations to K_{ATP} channel function were altered in response to Kir6.2 deletion (Fig. 2B), including long chain acyl-CoA dehydrogenase, lactate dehydrogenase A and B, glyceraldehyde-3-phosphate dehydrogenase, and triosephosphate isomerase [42–47], thereby validating the sensitivity and specificity of the employed proteomic approach.

Beyond verifying these previously identified K_{ATP} channel interactions, the high-throughput approach utilized here expanded the metabolism-related K_{ATP} channel-dependent subproteome (Fig. 3). Specifically, a total of 114 unique proteins were found to be altered in Kir6.2-KO hearts, following assignments for 63 of the 81 differentially expressed protein species [see Table S1 and S2 of Supporting Information]. Cellular metabolism was the primary function associated with 64% of identified proteins, accounting for 45 mitochondrial and 28 cytoplasmic metabolic proteins within the resolved K_{ATP} channel-dependent subproteome (Fig. 3). Complete ontological annotation revealed that the remaining 41 identified proteins form a metabolism-related infrastructure encompassing oxidoreductases (15 proteins), stress related chaperones (2), components of the proteasome (6), signaling regulation (5), transcription and translation (8), as well as cellular structure and scaffolding (6) (Fig. 4). Thus, this comprehensive protein identification and ontological stratification approach mapped a definitive set of 114 proteins in the setting of HTN, expanding by over an order of magnitude the resolved elements of the Kir6.2 interactome.

3.3 Kir6.2-dependent network assembly and topography

Network analysis was carried out to chart physiological and pathophysiological systems processes associated with the Kir6.2-dependent subproteome. The 114 identified proteins were integrated into a composite neighborhood comprised of 242 nodes linked by 1215 interactions or edges (Fig. 5). Network topology was not random, demonstrating a definitive nonstochastic property confirmed by examination of the interrelationship between node degree (k) and degree distribution (P[k]) (Fig. 5). The organized assemblage followed a power law distribution indicative of scale-free architecture, where $P(k) \sim k^{-\gamma}$, with $\gamma = 1.713 \pm 0.046$ (Fig. 5) falling within the predicted confidence range of biological networks [52,53]. The resolved K_{ATP} channel dependent network unmasked ontological linkage to modules of bioenergetic and metabolism related processes, integrating multiple energy producing, consuming and distributing pathways (Fig. 5). By encompassing vital hallmarks of inter-linked cardiovascular energy metabolism [69], the composite non-stochastic, metabolism-centric neighborhood provides an unbiased systems framework for predictive interrogation of K_{ATP} channel criticality in the setting of HTN.

3.4 Adverse outcomes predicted from the Kir6.2-dependent network

Criticality enables coordination of complex behaviors, balancing stability with adaptability [70]. Interrogation of the K_{ATP} channel-dependent network for links to a broad spectrum of 134 pathological conditions and toxicological pathways, curated in Ingenuity Pathways Knowledge Base, exclusively extracted three adverse effects: “Cardiac Damage”, “Cardiac Enlargement”, and “Cardiac Fibrosis” (Fig. 6A). This highly targeted cardiac-specific outcome with a likelihood of 1 in >2 000 000 of obtaining only these three outcomes at random ($1/134 \times 1/133 \times 1/132 = 1/[2.35 \times 10^6]$), without other significantly over-represented pathological or toxicological link-ages, indicated a critical role for K_{ATP} channels in

coordinating proper adaptive response to hypertensive stress load. The maladaptive response forecast was validated at both functional and structural levels. Specifically, in response to HTN, Kir6.2-KO ($n = 8$) compared to WT ($n = 8$) demonstrated poor cardiac muscle performance (Fig. 6B, left), an increase in heart to body weight ratios (Fig. 6B, right), and exaggerated collagen deposition (Fig. 6C), indicating damage, enlargement, and fibrosis, respectively. With HTN, heart contractile function was significantly impaired only in Kir6.2-KO, with a 32% decrease in cardiac output, in contrast to WT where no significant change was observed (Fig. 6B, left). Increased left ventricular mass in the setting of systemic HTN, a major predictor of poor outcome, was significantly greater in the Kir6.2-KO *versus* WT cohort (Fig. 6B, right). Moreover, Sirius red staining of left ventricular tissue revealed greater prevalence of noncontractile, collagen-rich fibrotic deposition in hypertensive Kir6.2-KO relative to WT in response to HTN (Fig. 6C). Thus, objective forecasting of severe adverse cardiac outcomes, predicted from the resolved Kir6.2-dependent sub-proteome network, establishes a role for K_{ATP} channels as molecular contributors to criticality, ensuring adaptability under pathophysiological hypertensive stress load.

4 Discussion

High blood pressure is a common cause of cardiovascular disease, yet there is marked variation in the susceptibility of hypertensive individuals to develop cardiomyopathy [1–9]. Why certain patients progress to overt heart failure while others do not, despite similar risk load, has been attributed to genomically predetermined homeostatic reserve [71]. In this regard, genetic divergence in stress-responsive K_{ATP} channels was recently implicated as a risk factor for transition from hypertensive stress to cardiac maladaptation [72], with knockout of the Kir6.2 channel pore precipitating severe heart failure when superimposed upon HTN [28]. However, the global molecular adaptation that occurs in response to myocardial K_{ATP} channel deficiency, and that underlies individual susceptibility for developing hypertensive cardiomyopathy, remains unknown.

The present study demonstrates that K_{ATP} channel deficit significantly remodels the cardiac proteome in HTN. Specifically, in a chronic hypertensive K_{ATP} channel knockout model, we identified a myocardial proteome of 114 altered proteins assembling into an interconnected, metabolism-centric K_{ATP} channel-dependent neighborhood. This resolved subproteome exposed a predilection for cardiomyopathy and onset of heart failure through unfavorable reorganization of the elucidated set of altered proteins and their expanded protein web. Dissecting the molecular fingerprint of K_{ATP} channel-dependent associations by comprehensive protein identification, ontological stratification, and predictive interrogation thus creates a systems framework tool to forecast outcome.

2-D gel separation coupled with nanoelectrospray linear IT tandem MS provided a high throughput, unbiased method to resolve and characterize the multiplicity of changes arising from the K_{ATP} channel-dependent subproteome in the hypertensive state [50–53,59]. High specificity protein cartography of the hypertensive K_{ATP} channel knockout heart displayed pronounced re-arrangement in cellular energetics (73 of 114 proteins), consistent with the proposed role for K_{ATP} channels as metabolic checkpoints supporting the adaptive, cardioprotective response to sustained hemodynamic stress [21,28]. In fact, over two-thirds of detected changes were down-regulated, in line with the notion that intact K_{ATP} channels contribute to functional metabolic integration within the heart [17,49,73]. Down-regulated proteins included creatine kinase, adenylate kinase, and lactate dehydrogenase isoforms, all previously recognized for their direct K_{ATP} channel linkages in support of cardiac homeostasis [35,39,42,43,47,48]. The remaining 41 altered members of the K_{ATP} channel-dependent subproteome encompassed oxido-reductases, stress-related chaperones, proteasome subunits, and proteins involved in signaling regulation, transcription and translation, as well as cellular

structure and scaffolding components. Here, unbiased large scale proteomic mining establishes the comprehensive nature of the K_{ATP} channel related metabolic infrastructure of the hypertensive heart.

Mapping of protein–protein relationships authenticated the primary impact on metabolic pathways, delineating the K_{ATP} channel-dependent subproteome within a functional neighborhood comprised of 242 proteins. The resolved interactome fulfilled criteria of nonstochastic topography based on indices of connectedness, including node degree (*k*) and degree distribution (P[*k*]), with the log–log plot of P[*k*] *versus k* fitting a power law distribution indicative of scale-free network topography [52]. Most biological systems display a scale-free organization, with disease-perturbed regulatory networks differing from their normal counterparts in functional prioritization [74,75]. Iterative systems interrogation of the K_{ATP} channel-dependent web prioritized only heart-specific adverse effects, *i.e.*, "Cardiac Damage", "Cardiac Enlargement", and "Cardiac Fibrosis", exposing a predisposition for development of cardiomyopathic traits specific to the hypertensive Kir6.2 KO proteome. Validating this maladaptive forecast, functional and structural phenotyping documented aggravated myocardial contractile performance associated with massive interstitial fibrosis and exaggerated left ventricular size, strong prognostic indices of poor outcome. Indeed, in experimental HTN, knockout of the *KCNJ11* gene, encoding the Kir6.2 pore-forming subunit of K_{ATP} channels, causes defective decoding of HTN-induced metabolic distress signals setting in motion pathological calcium overload and aggravated structural remodeling, ultimately precipitating organ failure and survival disadvantage [28]. In this way, the networked integration of proteins provides a systems understanding of pathophysiological processes associated with development of hypertensive cardiomyopathy in the setting of K_{ATP} channel deficiency.

In summary, this study provides the first proteomic profiling of K_{ATP} channel-deficient hypertensive hearts, expanding the understanding of molecular alterations caused by lack of a critical metabolic sensor during hemodynamic stress challenge. In contrast to the WT that tolerates hypertensive load, genetically compromised hearts devoid of the *KCNJ11*-encoded Kir6.2 K_{ATP} channel function engender unfavorable proteomic remodeling, revealing the metabolism-centric molecular substrate for pathologic stress-associated cardiovascular disease. In conjunction with the use of bioinformatic interrogation to predict adverse effects [53,76], the resolved subproteome unmasked risk for maladaptive cardiomyopathic outcome in the context of K_{ATP} channelopathy and environmental challenge. In view of *KCNJ11* genetic variants conferring cardiac disease risk [72,77], the present demonstration that K_{ATP} channels are critical for the proteomic response to hemodynamic load establishes a foundation to further investigate the role of these cardioprotective channels in predictive medicine.

Acknowledgments

The authors thank Dr. Satsuki Yamada for intra-surgical photography, Jonathan Nesbitt for technical expertise, and the Mayo Proteomics Research Center staff, particularly Benjamin Madden, Kenneth Johnson, Christopher Mason and Roman Zenka, for expert guidance in mass spectrometry and bioinformatic analysis. Support was provided by the National Institutes of Health, Marriott Heart Disease Research Program, Marriott Foundation, Ted Nash Long Life Foundation, and the Japanese Ministry of Education, Science, Sports, Culture and Technology. JZ holds a Mayo Graduate School fellowship. DKA is the recipient of a Marriott Individualized Medicine Career Development Award. AT holds the Marriott Family Professorship in Cardiovascular Research at Mayo Clinic.

Abbreviations

HTN
: hypertension

K_{ATP}

ATP-sensitive K^+

Kir6.2-KO

Kir6.2 knockout

WT

wild-type

References

1. Kostis JB. From hypertension to heart failure: update on the management of systolic and diastolic dysfunction. Am J Hypertens 2003;16:18S–22S. [PubMed: 14511898]
2. Krum H, Gilbert RE. Demographics and concomitant disorders in heart failure. Lancet 2003;362:147–158. [PubMed: 12867118]
3. Tocci G, Sciarretta S, Volpe M. Development of heart failure in recent hypertension trials. J Hypertens 2008;26:1477–1486. [PubMed: 18551026]
4. Rosamond W, Flegal K, Furie K, Go A, et al. Heart disease and stroke statistics -2008 update: a report from the American Heart Association statistics committee and stroke statistics subcommittee. Circulation 2008;117:e25–e146. [PubMed: 18086926]
5. Towbin JA, Bowles NE. The failing heart. Nature 2002;415:227–233. [PubMed: 11805847]
6. Susic D, Frohlich ED. The aging hypertensive heart: a brief update. Nat Clin Pract Cardiovasc Med 2008;5:104–110. [PubMed: 18223542]
7. Bell J. Predicting disease using genomics. Nature 2004;429:453–456. [PubMed: 15164070]
8. Chien KR. Stress pathways and heart failure. Cell 1999;98:555–558. [PubMed: 10490095]
9. Lifton RP, Gharavi AG, Geller DS. Molecular mechanisms of human hypertension. Cell 2001;104:545–556. [PubMed: 11239411]
10. Miki T, Seino S. Roles of K_{ATP} channels as metabolic sensors in acute metabolic changes. J Mol Cell Cardiol 2005;38:917–925. [PubMed: 15910876]
11. Nichols CG. K_{ATP} channels as molecular sensors of cellular metabolism. Nature 2006;440:470–476. [PubMed: 16554807]
12. Ashcroft FM. ATP-sensitive K^+ channels and disease: from molecule to malady. Am J Physiol Endocrinol Metab 2007;293:E880–E889. [PubMed: 17652156]
13. Bryan J, Muñoz A, Zhang X, Düfer M, et al. ABCC8 and ABCC9: ABC transporters that regulate K^+ channels. Pflugers Arch 2007;453:703–718. [PubMed: 16897043]
14. Inagaki N, Gonoi T, Clement JP, Namba N, et al. Reconstitution of IK_{ATP}: An inward rectifier subunit plus the sulfonylurea receptor. Science 1995;270:1166–1170. [PubMed: 7502040]
15. Inagaki N, Gonoi T, Clement JP, Wang CZ, et al. A family of sulfonylurea receptors determines the pharmacological properties of ATP-sensitive K^+ channels. Neuron 1996;16:1011–1017. [PubMed: 8630239]
16. Lorenz E, Terzic A. Physical association between recombinant cardiac ATP-sensitive K^+ channel subunits Kir6.2 and SUR2A. J Mol Cell Cardiol 1999;31:425–434. [PubMed: 10093054]
17. Alekseev AE, Hodgson DM, Karger AB, Park S, et al. ATP-sensitive K^+ channel channel/enzyme multimer: Metabolic gating in the heart. J Mol Cell Cardiol 2005;38:895–905. [PubMed: 15910874]
18. Zingman LV, Alekseev AE, Hodgson-Zingman DM, Terzic A. ATP-sensitive potassium channels: metabolic sensing and cardioprotection. J Appl Physiol 2007;103:1888–1893. [PubMed: 17641217]
19. Zingman LV, Hodgson DM, Alekseev AE, Terzic A. Stress without distress: homeostatic role for K_{ATP} channels. Mol Psychiatry 2003;8:253–254. [PubMed: 12660794]
20. Bienengraeber M, Olson TM, Selivanov VA, Kathmann EC, et al. *ABCC9* mutations identified in human dilated cardiomyopathy disrupt catalytic K_{ATP} channel gating. Nat Genet 2004;36:382–387. [PubMed: 15034580]
21. Kane GC, Liu XK, Yamada S, Olson TM, Terzic A. Cardiac K_{ATP} channels in health and disease. J Mol Cell Cardiol 2005;38:937–943. [PubMed: 15910878]
22. Zingman LV, Hodgson DM, Bast PH, Kane GC, et al. Kir6.2 is required for adaptation to stress. Proc Natl Acad Sci USA 2002;99:13278–13283. [PubMed: 12271142]

23. Liu XK, Yamada S, Kane GC, Alekseev AE, et al. Genetic disruption of Kir6.2, the pore-forming subunit of ATP-sensitive K^+ channel, predisposes to catecholamine-induced ventricular dysrhythmia. Diabetes 2004;53:S165–S168. [PubMed: 15561906]
24. Tong XY, Porter LM, Liu GX, Dhar-Chowdhury P, et al. Consequences of cardiac myocyte-specific ablation of K_{ATP} channels in transgenic mice expressing dominant negative Kir6 subunits. Am J Physiol Heart Circ Physiol 2006;291:H543–H551. [PubMed: 16501027]
25. Olson TM, Alekseev AE, Moreau C, Liu XK, et al. K_{ATP} channel mutation confers risk for vein of Marshall adrenergic atrial fibrillation. Nat Clin Pract Cardiovasc Med 2007;4:110–116. [PubMed: 17245405]
26. Reyes S, Kane GC, Miki T, Seino S, Terzic A. K_{ATP} channels confer survival advantage in cocaine overdose. Mol Psychiatry 2007;12:1060–1061. [PubMed: 18043710]
27. Kane GC, Behfar A, Yamada S, Perez-Terzic C, et al. ATP-sensitive K^+ channel knockout compromises the metabolic benefit of exercise training, resulting in cardiac deficits. Diabetes 2004;53:S169–S175. [PubMed: 15561907]
28. Kane GC, Behfar A, Dyer RB, O'Cochlain DF, et al. *KCNJ11* gene knockout of the Kir6.2 K_{ATP} channel causes maladaptive remodeling and heart failure in hypertension. Hum Mol Genet 2006;15:2285–2297. [PubMed: 16782803]
29. Kane GC, Lam CF, O'Cochlain F, Hodgson DM, et al. Gene knockout of the *KCNJ8*-encoded Kir6.1 K_{ATP} channel imparts fatal susceptibility to endotoxemia. FASEB J 2006;20:2271–2280. [PubMed: 17077304]
30. Yamada S, Kane GC, Behfar A, Liu XK, et al. Protection conferred by myocardial ATP-sensitive K^+ channels in pressure overload-induced congestive heart failure revealed in *KCNJ11* Kir6.2-null mutant. J Physiol 2006;577:1053–1065. [PubMed: 17038430]
31. Suzuki M, Sasaki N, Miki T, Sakamoto N, et al. Role of sarcolemmal K_{ATP} channels in cardioprotection against ischemia/reperfusion injury in mice. J Clin Invest 2002;109:509–516. [PubMed: 11854323]
32. Gumina RJ, Pucar D, Bast P, Hodgson DM, et al. Knockout of Kir6.2 negates ischemic preconditioning-induced protection of myocardial energetics. Am J Physiol Heart Circ Physiol 2003;284:H2106–H2113. [PubMed: 12598229]
33. Gumina RJ, O'Cochlain DF, Kurtz CE, Bast P, et al. K_{ATP} channel knockout worsens myocardial calcium stress load in vivo and impairs recovery in stunned heart. Am J Physiol Heart Circ Physiol 2007;292:H1706–H1713. [PubMed: 17189350]
34. Du Q, Jovanovic S, Clelland A, Sukhodub A, et al. Overexpression of SUR2A generates a cardiac phenotype resistant to ischemia. FASEB J 2004;20:1131–1141. [PubMed: 16770012]
35. Elvir-Mairena JR, Jovanovic A, Gomez LA, Alekseev AE, Terzic A. Reversal of the ATP-liganded state of ATP-sensitive K^+ channels by adenylate kinase activity. J Biol Chem 1996;271:31903–31908. [PubMed: 8943234]
36. Dzeja PP, Terzic A. Phosphotransfer reactions in the regulation of ATP-sensitive K^+ channels. FASEB J 1998;12:523–529. [PubMed: 9576479]
37. Bienengraeber M, Alekseev AE, Abraham MR, Carrasco AJ, et al. ATPase activity of the sulfonylurea receptor: A catalytic function for the K_{ATP} channel complex. FASEB J 2000;14:1943–1952. [PubMed: 11023978]
38. Zingman LV, Alekseev AE, Bienengraeber M, Hodgson DM, et al. Signaling in channel/enzyme multimers: ATPase transitions in SUR module gate ATP-sensitive K^+ conductance. Neuron 2001;31:233–245. [PubMed: 11502255]
39. Selivanov VA, Alekseev AE, Hodgson DM, Dzeja PP, Terzic A. Nucleotide-gated K_{ATP} channels integrated with creatine and adenylate kinases: amplification, tuning and sensing of energetic signals in the compartmentalized cellular environment. Mol Cell Biochem 2004;256:243–256. [PubMed: 14977185]
40. Park S, Lim BB, Perez-Terzic C, Mer G, Terzic A. Interaction of asymmetric *ABCC9*-encoded nucleotide binding domains determines K_{ATP} channel SUR2A catalytic activity. J Proteome Res 2008;7:1721–1728. [PubMed: 18311911]
41. Burke MA, Mutharasan RK, Ardehali H. The sulfonyl-urea receptor, an atypical ATP-binding cassette protein, and its regulation of the K_{ATP} channel. Circ Res 2008;102:164–176. [PubMed: 18239147]

42. Carrasco AJ, Dzeja PP, Alekseev AE, Pucar D, et al. Adenylate kinase phosphotransfer communicates cellular energetic signals to ATP-sensitive potassium channels. Proc Natl Acad Sci USA 2001;98:7623–7628. [PubMed: 11390963]
43. Crawford RM, Ranki HJ, Botting CH, Budas GR, Jovanovic A. Creatine kinase is physically associated with the cardiac ATP-sensitive K^+ channel *in vivo*. FASEB J 2002;16:102–104. [PubMed: 11729098]
44. Dhar-Chowdhury P, Harrell MD, Han SY, Jankowska D, et al. The glycolytic enzymes, glyceraldehyde-3-phosphate dehydrogenase, triosephosphate isomerase, and pyruvate kinase are components of the K_{ATP} channel macromolecular complex and regulate its function. J Biol Chem 2005;280:38464–38470. [PubMed: 16170200]
45. Jovanovic S, Du Q, Crawford RM, Budas GR, et al. Glyceraldehyde 3-phosphate dehydrogenase serves as an accessory protein of the cardiac sarcolemmal K_{ATP} channel. EMBO Rep 2005;6:848–852. [PubMed: 16082386]
46. Liu GX, Hanley PJ, Ray J, Daut J. Long-chain acyl-coenzyme A esters and fatty acids directly link metabolism to K_{ATP} channels in the heart. Circ Res 2001;88:918–924. [PubMed: 11349001]
47. Abraham MR, Selivanov VA, Hodgson DM, Pucar D, et al. Coupling of cell energetics with membrane metabolic sensing: Integrative signaling through creatine kinase phosphotransfer disrupted by M-CK gene knock-out. J Biol Chem 2002;277:24427–24434. [PubMed: 11967264]
48. Crawford RM, Budas GR, Jovanovic S, Ranki HJ, et al. M-LDH serves as a sarcolemmal K_{ATP} channel subunit essential for cell protection against ischemia. EMBO J 2002;21:3936–3948. [PubMed: 12145195]
49. Hodgson DM, Zingman LV, Kane GC, Perez-Terzic C, et al. Cellular remodeling in heart failure disrupts K_{ATP} channel-dependent stress tolerance. EMBO J 2003;22:1732–1742. [PubMed: 12682006]
50. Hartwell LH. From molecular to modular cell biology. Nature 1999;402:C47–C52. [PubMed: 10591225]
51. Kitano H. Computational systems biology. Nature 2002;420:206–210. [PubMed: 12432404]
52. Barabási AL, Oltvai ZN. Network biology: understanding the cell's functional organization. Nat Rev Genet 2004;5:101–113. [PubMed: 14735121]
53. Weston AD, Hood L. Systems biology, proteomics, and the future of health care: toward predictive, preventative, and personalized medicine. J Proteome Res 2004;3:179–196. [PubMed: 15113093]
54. Miki T, Nagashima K, Tashiro F, Kotake K, et al. Defective insulin secretion and enhanced insulin action in K_{ATP} channel-deficient mice. Proc Natl Acad Sci USA 1998;95:10402–10406. [PubMed: 9724715]
55. Suzuki M, Li RA, Miki T, Uemura H, et al. Functional roles of cardiac and vascular ATP-sensitive potassium channels clarified by Kir6.2-knockout mice. Circ Res 2001;88:570–577. [PubMed: 11282890]
56. Arrell DK, Neverova I, Fraser H, Marbán E, Van Eyk JE. Proteomic analysis of pharmacologically preconditioned cardiomyocytes reveals novel phosphorylation of myosin light chain 1. Circ Res 2001;89:480–487. [PubMed: 11557734]
57. Arrell DK, Elliott ST, Kane LA, Guo Y, et al. Proteomic analysis of pharmacological preconditioning: Novel protein targets converge to mitochondrial metabolism pathways. Circ Res 2006;99:706–714. [PubMed: 16946135]
58. Arrell DK, Niederländer NJ, Perez-Terzic C, Behfar A, Terzic A. Embryonic stem cell cardiac differentiation: A proteomic perspective. Adv Mol Med 2006;2:149–156.
59. Arrell DK, Niederländer NJ, Faustino RS, Behfar A, Terzic A. Cardioinductive network guiding stem cell differentiation revealed by proteomic cartography of tumor necrosis factor alpha-primed endodermal secretome. Stem Cells 2008;26:387–400. [PubMed: 17991915]
60. Behfar A, Perez-Terzic C, Faustino RS, Arrell DK, et al. Cardiopoietic programming of embryonic stem cells for tumor-free heart repair. J Exp Med 2007;204:405–420. [PubMed: 17283208]
61. Perkins DN, Pappin DJC, Creasy DM, Cottrell JS. Probability-based protein identification by searching sequence databases using mass spectrometry data. Electrophoresis 1999;20:3551–3567. [PubMed: 10612281]

62. Link AJ, Eng J, Schieltz DM, Carmack E, et al. Direct analysis of protein complexes using mass spectrometry. Nat Biotechnol 1999;17:676–682. [PubMed: 10404161]
63. Assenov Y, Ramírez F, Schelhorn SE, Lengauer T, Albrecht M. Computing topological parameters of biological networks. Bioinformatics 2008;24:282–284. [PubMed: 18006545]
64. Barabási AL, Albert R. Emergence of scaling in random networks. Science 1999;286:509–512. [PubMed: 10521342]
65. Jeong H, Tombor B, Albert R, Oltavi ZN, Barabási AL. The large-scale organization of metabolic networks. Nature 2000;407:651–654. [PubMed: 11034217]
66. Anderson TW, Darling DA. Asymptotic theory of certain “goodness-of-fit” criteria based on stochastic processes. Ann Math Stat 1952;23:193–212.
67. Newman MEJ. The structure and function of complex networks. SIAM Rev 2003;45:167–256.
68. Weber KT. Aldosterone in congestive heart failure. N Engl J Med 2001;345:1689–1697. [PubMed: 11759649]
69. Weiss JN, Yang L, Qu Z. Network perspectives of cardiovascular metabolism. J Lipid Res 2006;47:2355–2366. [PubMed: 16946414]
70. Nykter M, Price ND, Aldana M, Ramsey SA, et al. Gene expression dynamics in the macrophage exhibit criticality. Proc Natl Acad Sci USA 2008;105:1897–1900. [PubMed: 18250330]
71. Bleumink GS, Schut AF, Sturkenboom MC, Deckers JW, et al. Genetic polymorphisms and heart failure. Genet Med 2004;6:465–474. [PubMed: 15545741]
72. Reyes S, Terzic A, Mahoney DW, Redfield MM, et al. K_{ATP} channel polymorphism is associated with left ventricular size in hypertensive individuals: a large-scale community-based study. Hum Genet 2008;123:665–667. [PubMed: 18504616]
73. Dzeja PP, Terzic A. Phosphotransfer networks and cellular energetics. J Exp Biol 2003;206:2039–2047. [PubMed: 12756286]
74. Hood L, Heath JR, Phelps ME, Lin B. Systems biology and new technologies enable predictive and preventative medicine. Science 2004;306:640–643. [PubMed: 15499008]
75. Loscalzo J, Kohane I, Barabási AL. Human disease classification in the postgenomic era: a complex systems approach to human pathobiology. Mol Syst Biol 2007;3:124. [PubMed: 17625512]
76. Arrell DK, Niederländer NJ, Perez-Terzic C, Chung S, et al. Pharmacoproteomics: advancing the efficacy and safety of regenerative therapeutics. Clin Pharmacol Ther 2007;82:316–319. [PubMed: 17671447]
77. Sattiraju S, Reyes S, Kane GC, Terzic A. K_{ATP} channel pharmacogenomics: from bench to bedside. Clin Pharmacol Ther 2008;83:354–357. [PubMed: 17957187]

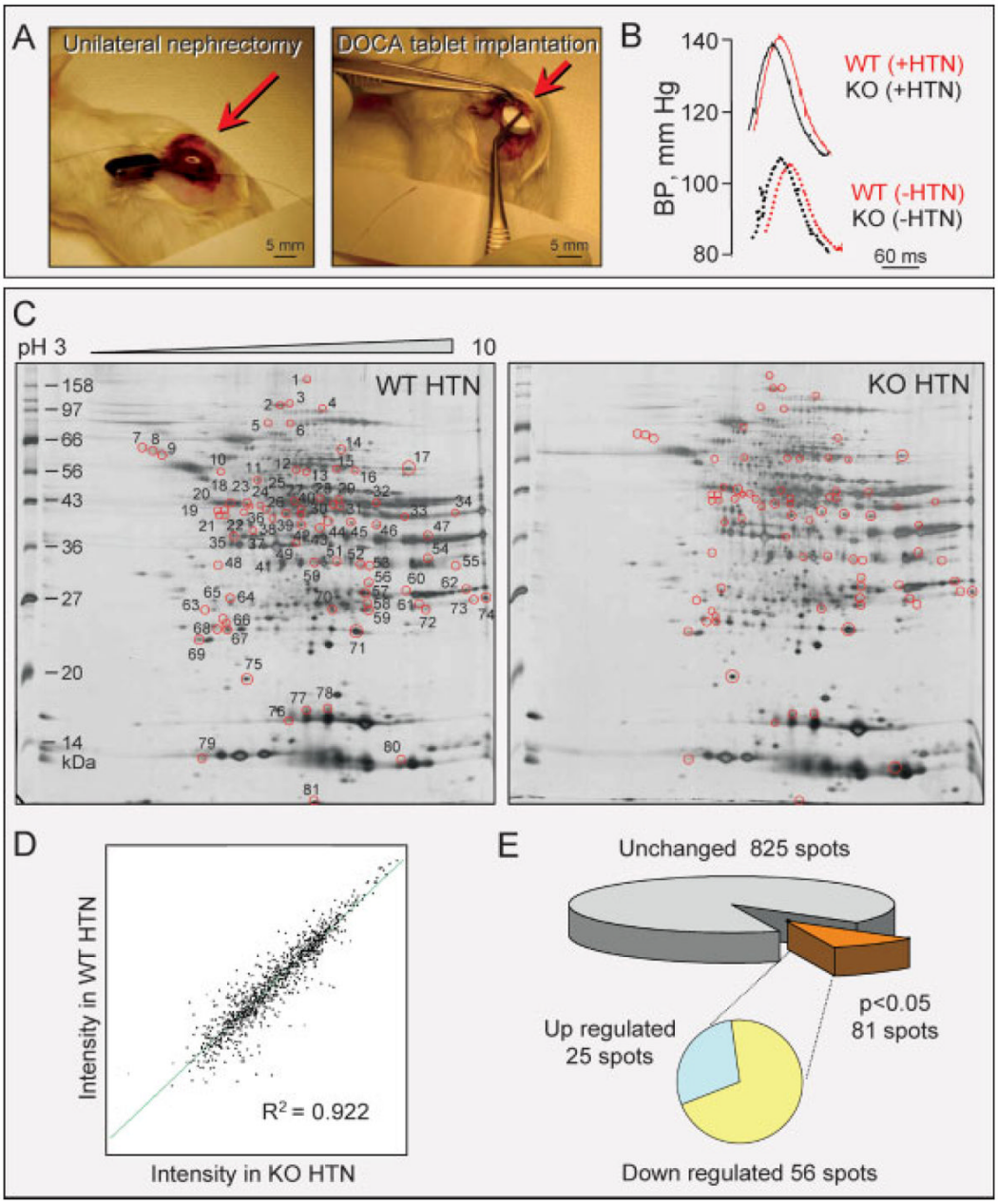

Figure 1.

Impact of Kir6.2 KO on the ventricular proteome in HTN. (A) Unilateral nephrectomy (left) and implantation of deoxy-corticosterone acetate (DOCA) releasing tablet (right) were implemented in WT and age/sex-matched Kir6.2-KO mice to induce HTN through volume overload. (B) Blood pressure measurements revealed significant yet comparable HTN at 14 days of volume overload in WTand Kir6.2-KO. (C) Representative 2-D gels of left ventricular cytoplasmic protein extracts (100 μg per gel) from hypertensive WT (WT HTN) and Kir6.2-KO (KO HTN) mice resolved by pH 3–10 IEF/12.5% SDS–PAGE. Differentially expressed spots are circled, and numbered on the WT HTN gel to cross-reference with the corresponding protein identities determined by LTQ-Orbitrap MS/MS analysis of excised tryptic digests (listed in Fig. 3 and Fig. 4 and Table S1 and S2 of Supporting Information). (D) Average

normalized intensities of matching protein spots from WT HTN and Kir6.2-KO HTN gels indicated a high level of gel-to-gel reproducibility and correlation ($R^2 = 0.922$) across cohorts. (E) Statistical analysis comparing WT to Kir6.2-KO gel densitometric spot quantitation revealed a subset of 81 spots that differed in Kir6.2-KO extracts ($p<0.05$), with 56 down-regulated and 25 up-regulated protein species.

A

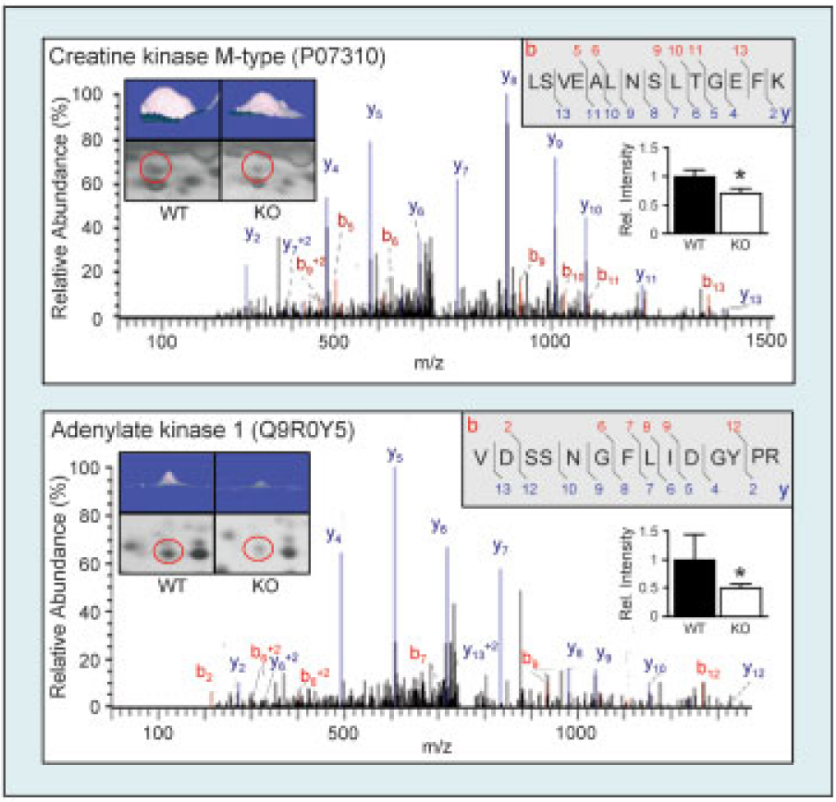

B

Protein name	Accession number	Fold change	Metabolic process
Adenylate kinase 1	Q9R0Y5	-2.50	Energy shuttle
Creatine kinase-M	O88587	-1.23	Energy shuttle
Lactate dehydrogenase A	P06151	-1.65	Energy shuttle
Lactate dehydrogenase B	P16125	-2.76	Glycolysis
Glyceraldehyde-3-phosphate dehydrogenase	P16858	2.62	Glycolysis
Long chain acyl-CoA dehydrogenase	P51174	-1.32	Fatty acid synthesis

Figure 2.

Metabolic enzymes associated with K_{ATP} channel function are among the differentially affected subproteome. (A) Representative LTQ-Orbitrap MS/MS product ion spectra obtained for spots #40 (upper) and #67 (lower), modified from BioWorks 3.2 to indicate detected b-ions in red and y-ions in blue, with corresponding peptide sequences of the identified proteins, creatine kinase M-type and adenylate kinase 1 (upper right insets). Spots are shown for comparison by 2-D gel region enlargement (circled in red) and 3-D rendering (upper left insets), with relative spot intensities indicated in the histogram (middle right insets). (B) A number of additional metabolic enzymes with known association to K_{ATP} channels were significantly altered in Kir6.2-KO hypertensive hearts.

Protein Name (Node Symbol) Spot Number(s)	Swiss- Prot Accession	Mascot Score	Unique Peptides	Sequence Cov. (%)	Predicted Mr	Predicted pI	Fold Change		
2,4-dienoyl-CoA reductase (Decr1) **50**	Q9CQ62	137	3	17	32451	8.78	-1.53	Mitochondrial	Metabolism
28S ribosomal protein S7 (Mrps7) **74**	Q80X85	87	2	10	24072	9.72	-1.55		
2-oxoglutarate dehydrogenase E1 component (Ogdh) **3**	Q60597	229	6	12	111840	6.05	-4.64		
3,2-trans-enoyl-CoA isomerase (Dci) **60**	P42125	42	1	7	29111	7.77	-9.13		
3-ketoacyl-CoA thiolase (Acaa2) **28**, **29, 32**	Q8BWT1	604	12	63	41858	8.33	1.55		
3-ketoacyl-CoA thiolase A, peroxisomal (Acaa1a) **34**	Q921H8	78	2	8	41242	8.63	2.46		
3-hydroxyisobutyryl-CoA hydrolase (Hibch) **42**	Q8QZS1	983	16	49	39239	6.24	-1.43		
Aconitate hydratase (Aco2) **4**	Q99KI0	101	2	4	82464	7.40	-3.73		
Acetyl-CoA acetyltransferase (Acat1) **31**	Q8QZT1	224	4	20	41414	8.18	6.80		
Acyl-coenzyme A thioesterase 1 (Acot1) **58**	O55137	57	1	5	46136	6.12	-1.63		
Acyl-coenzyme A thioesterase 2 (Acot2) **27**	Q9QYR9	589	12	40	44934	6.14	-1.78		
Aspartate aminotransferase (Got2) **33**, **34**	P05202	726	14	14	44579	8.89	1.32		
ATP synthase mitochondrial F1 complex assembly factor 2 (Atpaf2) **64**	Q91YY4	139	3	14	28503	5.27	-1.37		
ATP synthase subunit alpha (Atap5a1) **15**	Q03265	90	1	2	55310	8.28	1.95		
Branched-chain-amino-acid aminotransferase (Bcat2) **44**, **41**, **46**, **45**	O35855	284	6	22	41176	7.70	1.95		
Citrate synthase (Cs) **28**, **32**, **29**	Q9CZU8	671	15	33	49014	8.21	-2.96 1.96		
Cytochrome c, somatic (Cyc) **74**	P62897	193	5	39	11474	9.61	-1.55		
Coproporphyrinogen III oxidase (Cox) **43**	P36552	99	3	13	39679	6.47	-3.04		
Creatine kinase, sarcomeric (Ckmt1) **29**,**32**	Q6P8J7	1231	24	62	43387	7.72	2.17		
Dihydrolipoyllysine-residue succinyltransferase component of 2-oxoglutarate dehydrogenase complex (Dlst) **11**, **25**	Q9D2G2	480	11	21	41470	5.98	-6.93		
Electron transfer flavoprotein subunit alpha (Etfa) **50**, **51**, **52**, **53**	Q99LC5	489	9	26	32366	7.10	-1.67		
Electron transfer flavoprotein subunit beta (Etfb) **60**, **62**	Q9DCW4	171	5	20	27492	8.29	-2.39 1.66		
Elongation factor G 1 (Efg1) **5**	Q8K0D5	129	3	5	79422	5.87	-3.76		
Enoyl-CoA hydratase (Echs1) **70**	Q8BH95	143	3	15	28475	7.78	-1.67		
ES1 protein homolog (Es1) **58**, **59**, **70**	Q9D172	199	5	28	23920	7.31	-1.30		
Fumarate hydratase (Fh) **31**	P97807	62	1	4	49935	7.88	6.79		
Glutamate dehydrogenase 1 (Glud1) **12**	P26443	45	1	3	55913	6.71	-2.55		
Glutaryl-CoA dehydrogenase (Gcdh) **32**	Q60759	155	4	15	43737	6.60	2.17		
GTP:AMP phosphotransferase (Ak3) **74**	Q9WTP7	379	8	38	25295	8.88	-1.55		
Hydroxyacyl-coenzyme A dehydrogenase (Hadh) **50**, **52**, **53**, **54**	Q61425	247	6	17	32995	8.26	-2.37		
Isochorismatase domain-containing protein 2A (Isoc2a) **71**	P85094	349	4	40	16021	6.34	1.20		
Isocitrate dehydrogenase [NADP] (Idha3A) **21**	Q9D6R2	72	1	16	36707	5.60	-3.76		
Isovaleryl-CoA dehydrogenase (Ivd) **25**	Q9JHI5	290	5	15	42971	6.29	-2.16		
Long-chain specific acyl-CoA dehydrogenase (Acadl) **25**, **39**, **27**, **40**,**41**, **28**	P51174	1031	23	48	44627	6.50	-1.32		
Malate dehydrogenase (Mdh2) **47**, **54, 55**	P08249	465	11	41	33139	8.55	2.62 -3.63		
Medium-chain specific acyl-CoA dehydrogenase (Acadm) **25**, **27**, **40**, **28**, **30**, **32**	P45952	426	9	28	43593	7.69	-1.26 2.19		
Methylcrotonoyl-CoA carboxylase beta chain (Mccc2) **32**	Q3ULD5	44	1	3	54718	7.25	2.17		
Methylmalonyl-CoA mutase (Mut) **5**	P16332	450	11	18	79360	6.08	-3.76		
Pyruvate dehydrogenase E1 component subunit alpha (Pdha) **25**, **27**, **28**, **40**	P35486	285	6	24	40181	6.78	-1.24		
Pyruvate dehydrogenase E1 component subunit beta (Pdhb) **35**	P35486	134	2	9	35768	5.39	-1.62		
Short/branched chain specific acyl-CoA dehydrogenase (Acadsb) **26**, **39**	Q9DBL1	112	2	9	44041	6.06	-1.60		
Short-chain specific acyl-CoA dehydrogenase (Acads) **39**, **40**, **41**	Q07417	963	16	51	42231	7.12	-1.50		
Succinyl-CoA ligase [ADP-forming] beta-chain (Sucla2) **19**	Q9Z2I9	183	4	12	44422	5.33	-37.94		
Succinyl-CoA ligase [GDP-forming] beta-chain (Suclg2) **19**	Q9Z2I8	62	2	6	42695	5.42	-37.94		
3-hydroxyacyl-CoA dehydrogenase type-2 (Hsd17b10) **58**, **61**, **72**, **74**	O08756	368	6	37	27287	8.56	-2.67		
Aspartate aminotransferase (Got1) **40**, **41**	P05201	1179	23	59	44579	8.97	-1.52	Cytoplasmic	
5'-AMP-activated protein kinase subunit gamma-1 (Prkag1) **43**	O54950	347	7	30	37520	6.64	-3.04		
Adenylate kinase isoenzyme 1 (Ak1) **66**, **67**, **68**	Q9R0Y5	322	6	39	21540	5.67	-2.50		
Alpha-enolase (Eno1) **46**	P17182	78	1	4	47010	6.36	2.31		
Aminoacylase-1 (Acy1) **25**	Q99JW2	121	3	8	45781	5.89	-2.17		
Calpain small subunit 1 (Css1) **64**	O88456	141	4	24	28463	5.41	-1.37		
Catechol O-methyltransferase (Comt) **66**	O88587	79	2	18	29496	5.52	-2.24		
Creatine kinase M-type (Ckm) **27**, **28**, **40**	P07310	669	12	36	43045	6.58	-1.23		
Fructose-bisphosphate aldolase A (Aldoa) **31**, **33**, **34**	P05064	807	15	63	39225	8.40	1.50		
Fumarylacetoacetase (Fah) **30**, **31**	P35505	424	8	32	46104	6.92	1.95		
Glucose- 6- phosphate isomerase (Gpi) **17**	P06745	578	14	15	62636	8.18	-6.35		
Glyceraldehyde-3-phosphate dehydrogenase (Gapdh) **47**	P16858	219	6	17	35679	8.45	2.62		
Glycerol-3-phosphate dehydrogenase 1-like protein (Gpd1l) **42**	Q3ULJ0	71	2	9	38226	6.34	-1.43		
Glycogen phosphorylase, muscle form (Pygm) **4**	Q9WUB3	564	13	18	97155	6.65	-3.73		
L-lactate dehydrogenase A chain (Ldha) **52**	P06151	235	5	17	36367	7.76	-1.65		
L-lactate dehydrogenase B chain (Ldhb) **35**, **37**	P16125	506	10	32	36441	5.70	-2.76		
Malate dehydrogenase, cytoplasmic (Mdh1) **38**	P14152	202	4	15	36380	6.16	-2.15		
Mannose-6-phosphate isomerase (Mpi) **23**	Q924M7	162	3	12	46575	5.62	4.86		
Nucleoside diphosphate kinase A (Ndka) **77**	P15532	34	1	25	17208	6.84	1.32		
Phosphoglycerate kinase 1 (Pgk1) **28**,**32**	P09411	361	8	27	44419	8.02	-2.90 2.17		
Phosphoglycerate mutase 2 (Pgam) **62**	O70250	449	9	37	28696	8.65	1.66		
Protein NDRG2 (Ndrg2) **19**	Q9QYG0	58	1	3	40789	5.23	-37.94		
Serine/threonine-protein phosphatase 2A regulatory subunit B' (Ppp2r4) **38**	P58389	145	4	12	36710	5.95	-2.15		
Serine/threonine-protein phosphatase PP1-beta catalytic subunit (Ppp1cb) **37**	P62141	50	1	3	37056	5.85	-8.73		
Triosephosphate isomerase (Tpi1) **58**	P17751	291	6	32	26581	7.09	-1.63		
UTP--glucose-1-phosphate uridylyltransferase 2 (Ugp2) **15**, **16**	Q91ZJ5	962	20	44	56848	7.17	1.67		
Zinc-binding alcohol dehydrogenase domain-containing protein 1 (Zadh1) **21**	Q8VDQ1	269	6	25	38054	5.38	-3.76		
Zinc-binding alcohol dehydrogenase domain-containing protein 2 (Zadh2) **38**, **41**	Q8BGC4	110	2	9	40529	7.01	-1.66		

Figure 3.

Metabolism is the predominant function of Kir6.2-KO proteins differentially altered in response to HTN. Significantly altered spots identified by LTQ-Orbitrap MS/MS analysis and functionally categorized by their respective Swiss-Prot ontological annotations were primarily associated with metabolism related processes, with 45 and 28 proteins involved in mitochondrial or cytoplasmic metabolism, respectively. Protein names are listed with corresponding spot numbers to locate their 2-D gel position(s) in Fig. 1, and with Swiss-Prot gene names for locating them in the protein interaction network in Fig. 5. Protein Mascot score, number of unique identified peptides, % sequence cov. (coverage), predicted M_r and p*I* for each protein (following expected post-translational processing, *e.g.*, removal of a

mitochondrial signal peptide), and fold change (KO *vs*. WT) are indicated. For proteins detected in more than one spot, the maximum score and corresponding number of unique peptides are reported. Fold change was calculated as described in experimental procedures, and for proteins detected in both increasing and decreasing spots, both values are indicated. Complete MS/MS data for all proteins is outlined in Table S1 and S2 of Supporting Information.

Protein Name (Node Symbol) Spot Number(s)	Swiss- Prot Accession	Mascot Score	Unique Peptides	Sequence Cov. (%)	Predicted Mr	Predicted pI	Fold Change	
Aldose reductase-related protein 1(Akr1b7) **50**	P21300	35	1	4	35857	6.85	-1.53	Oxidoreductase
Alcohol dehydrogenase [NADP+] (Akr1a1) **43**	Q9JII6	259	6	27	36456	6.87	-3.04	
Aflatoxin B1 aldehyde reductase member 2 (Akr7a2) **42**	Q8CG76	155	3	10	40598	8.36	-1.43	
Carbonyl reductase [NADPH] (Cbr1) **54**	P48758	190	4	17	30510	8.53	-3.63	
Glutathione S-transferase Mu 1 (Gstm1) **61**, **58**, **74**, **72**	P10649	909	17	61	25839	8.14	-1.95	
Glutathione S-transferase Mu 2 (Gstm2) **59**	P15626	171	4	20	25586	7.31	-1.50	
Glyoxylate reductase/hydroxypyruvate reductase (Grhpr) **43**	Q91Z53	296	7	30	35329	7.57	-3.04	
Nicotinamide mononucleotide adenylyltransferase 3 (Nmnat3) **61**, **72**, **74**	Q99JR6	88	2	5	27703	8.71	-2.10	
Peroxiredoxin-1 (Prdx1) **71**	P35700	343	7	35	22177	8.26	1.20	
Peroxiredoxin-2 (Prdx2) **69**	Q61171	241	5	35	21647	5.20	-1.50	
Peroxiredoxin-5 (Prdx5) **76**, **77**, **78**	P99029	119	3	23	17015	7.70	1.50	
Sepiapterin reductase (Spr) **64**	Q64105	320	5	29	27883	5.59	-1.37	
Superoxide dismutase [Mn] (Sod2) **71**	P09671	777	15	51	22222	7.3	-1.55	
Thioredoxin-dependent peroxide reductase (Prdx3) **70**	P20108	67	1	5	21565	5.73	-1.67	
Thioredoxin-like protein 2 (PKC-interacting cousin of thioredoxin) (Glrx3) **21**	Q9CQM9	256	5	23	37647	5.43	-3.76	
Actin, alpha cardiac muscle 1 (Actc1) **19**	P68033	46	1	2	41992	5.24	-37.94	Cytostructure/ Scaffolding
Actin-related protein 2/3 complex subunit 2 (Arpc2) **50**	Q9CVB6	67	3	6	34357	6.84	-1.53	
Dynamin-1-like protein (Dnml1) **6**	Q8K1M6	125	3	6	82658	6.61	-7.15	
Myoglobin (Mb) **76**, **77**, **78**	P04247	484	8	63	16938	7.23	1.50	
Myosin light polypeptide 3 (Myl3) **63**	P09542	527	11	63	22290	5.03	-4.00	
Protein NipSnap2 (Gbas) **61**, **73**, **74**	O55126	540	12	34	32933	9.31	-1.88	
Hspb6 (Hspb6) **75**	Q5EBG6	188	3	38	17521	5.64	1.42	Chap.
Hsp70-binding protein 1 (HspBP1) **19**	Q99P31	122	3	8	70871	5.37	-37.94	
26S protease regulatory subunit S10B (Psmc6) **30**, **31**	P62334	378	10	3	44042	7.25	-1.61	Proteasome/ Degradation
26S proteasome non-ATPase regulatory subunit 13 (Psmd13) **36**	Q9WVJ2	64	2	6	42809	5.46	-1.86	
26S proteasome non-ATPase regulatory subunit 7 (Psmd7) **42**	P26516	77	1	5	36409	6.31	-1.43	
Proteasome subunit beta type 6 precursor (Psmb6) **68**	Q60692	99	2	9	21997	4.99	-114.45	
Ubiquitin (Ubb) **81**	P62991	245	6	68	8565	6.56	-3.18	
Annexin A1 (Anxa1) **43**	P10107	690	12	47	38603	7.15	-3.04	Signaling Regulation
Cysteine-rich protein 2 (Crip2) **74**	Q9DCT8	99	2	23	22727	8.94	-1.55	
ELAV-like protein 1 (Elavl1) **74**	P70372	110	2	7	36069	9.23	-1.55	
Lysophosphatidic acid phosphatase type 6 precursor (Acp6) **27**	Q8BP40	380	6	19	44789	6.58	-1.78	
Proto-oncogene C-crk (p38) (Crk) **35**	Q64010	122	2	9	33815	5.38	-1.62	
GTP-binding nuclear protein Ran (Ran) **70**	P62827	173	4	25	24292	7.20	-1.67	Transcription/ Translation
Guanine nucleotide-binding protein subunit beta 2-like 1 (Gnb2l1) **53**	P68040	56	1	3	34946	7.57	-32.71	
Elongation factor 1-alpha 2 (Eef1a2) **74**	P62631	33	1	2	50454	9.11	-1.67	
Elongation factor 2 (Eef2) **4**	P58252	721	15	23	95183	6.42	-1.65	
Elongation factor Tu (Eftu) **40**	Q8BFR5	115	3	12	44971	6.20	-1.43	
Translation initiation factor eIF-2B subunit beta (Eif2b2) **38**	Q99LD9	56	1	4	38898	5.82	-2.15	
Protein LRP16 (Macrod1) **58**, **61**, **72**	Q922B1	90	2	10	35295	9.07	-2.83	
Phosphatidylethanolamine-binding protein 1 (Pebp1) **69**	P70296	187	3	28	20699	5.19	-1.55	

Figure 4.

Remaining Kir6.2-KO proteins differentially altered in response to HTN comprise a metabolism infrastructure related module. Significantly altered spots identified by LTQ-Orbitrap MS/MS analysis included 41 proteins, and functionally categorized by their respective Swiss-Prot ontological annotations as oxidoreductases, cytostructure, and scaffolding proteins, stress related chaperones, proteasome, and degradation components, and elements of signaling regulation, and transcription and translation. Protein names are listed with corresponding spot numbers to locate their 2-D gel position(s) in Fig. 1, and with Swiss-Prot gene names for locating them in the protein interaction network in Fig. 5. Protein Mascot score, number of unique identified peptides, % sequence cov. (coverage), predicted M_r and p*I* for each protein (following expected post-translational processing, *e.g.*, removal of a mitochondrial signal peptide), and fold change (KO *vs.* WT) are indicated. Fold change was calculated as described in experimental procedures. Complete MS/MS data for all proteins is outlined in Table S1 and S2 of Supporting Information.

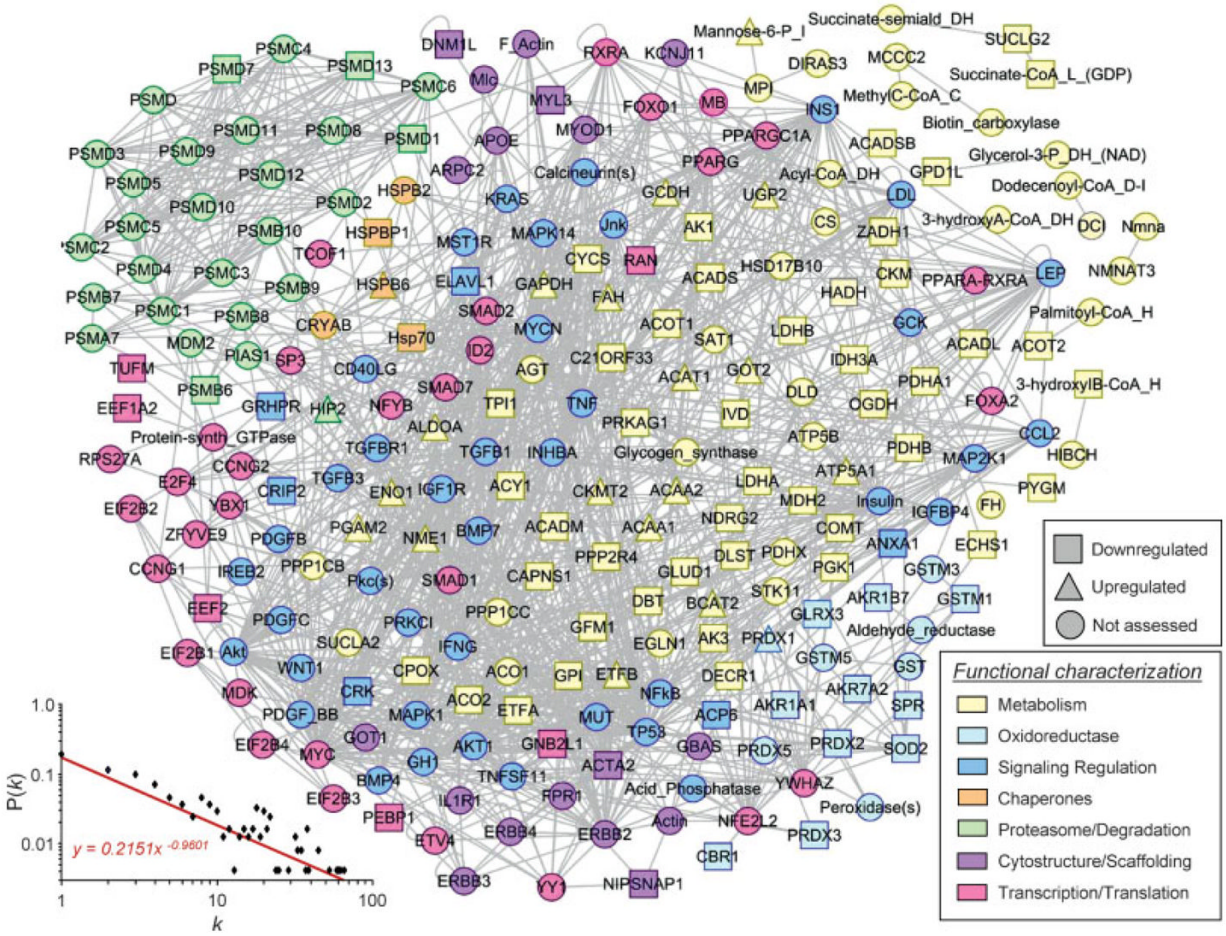

Figure 5.

Kir6.2-dependent protein–protein interaction network in HTN. The 114 differentially expressed proteins of the Kir6.2-dependent subproteome were submitted to Ingenuity Pathways Analysis as focus nodes, generating a 242 protein interaction network. Nodes are listed by Swiss-Prot gene names. Nodes are colored to correspond to functional categorization, while node shape indicates directionality of expression level change, unless the protein was not detected during proteomic analysis (legends, lower right). A plot of degree distribution (P [*k*]) *versus* degree (*k*) followed a power law distribution, indicating a scale free, nonstochastic network architecture (lower left).

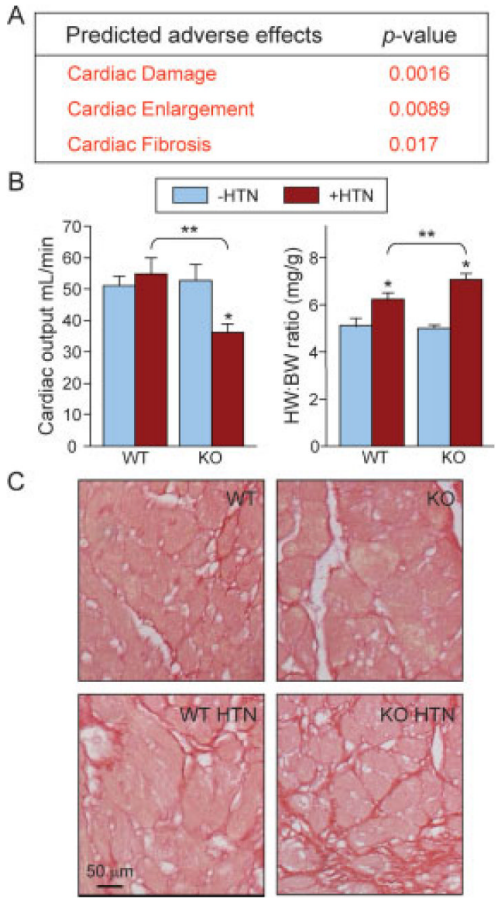

Figure 6.

Functional validation of adverse outcomes predicted from the Kir6.2-dependent network. (A) Interrogation of the K_{ATP} channel-dependent proteome for existing toxicological pathways in Ingenuity Pathways Knowledge Base revealed three statistically significant adverse effects: “Cardiac Damage”, “Cardiac Enlargement”, and “Cardiac Fibrosis”. Each of these predicted adverse effects was confirmed *in vivo* by (B) marked reduction of cardiac function as measured by cardiac output and increased cardiac mass measured by normalized heart to body weight (HW:BW) and (C) cardiac fibrosis as illustrated by Sirius red staining of increased collagen deposition (* $p<0.05$, −HTN *vs.* +HTN; ** $p<0.05$, WT +HTN *vs.* KO +HTN).